



High-speed tomography under extreme conditions at the PSICHE beamline of the SOLEIL Synchrotron

E. Boulard,^{a,b*} A. King,^a N. Guignot,^a J.-P. Deslandes,^a Y. Le Godec,^b J.-P. Perrillat,^c A. Clark,^b G. Morard^b and J.-P. Itié^a

^aSynchrotron SOLEIL, L'Orme des Merisiers, 91192 St Aubin, France, ^bSorbonne Université, Muséum National d'Histoire Naturelle, UMR CNRS 7590, IRD, Institut de Minéralogie, Physique des Matériaux et Cosmochimie – IMPMC, 4 Place Jussieu, 75005 Paris, France, and ^cLaboratoire de Géologie de Lyon, UMR CNRS 5276, Université Claude Bernard Lyon 1, ENS de Lyon, 69622 Villeurbanne, France. *Correspondence e-mail: egl.boulard@gmail.com

Received 15 December 2017

Accepted 26 March 2018

Edited by V. Favre-Nicolin, CEA and Université Joseph Fourier, France

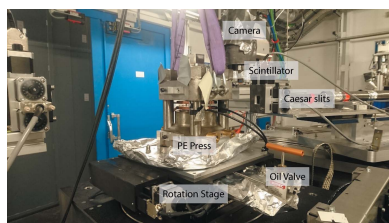
Keywords: X-ray absorption tomography; high pressure; melt.

In situ microtomography at high pressure and temperature has developed rapidly in the last decade, driven by the development of new high-pressure apparatus. It is now routinely possible to characterize material under high pressure with acquisition times for tomograms of the order of tens of minutes. Here, advantage was taken of the possibility to combine the use of a pink beam projected through a standard Paris–Edinburgh press in order to demonstrate the possibility to perform high-speed synchrotron X-ray tomography at high pressure and temperature allowing complete high-resolution tomograms to be acquired in about 10 s. This gives direct visualization to rapidly evolving or unstable systems, such as flowing liquids or reacting components, and avoids assumptions in the interpretation of quenched samples. Using algebraic reconstruction techniques allows the missing angle artefacts that result from the columns of the press to be minimized.

1. Introduction

Complex heterogeneous structures occur naturally at various length scales and under a vast range of conditions and modulate material properties and behaviour. The response of these heterogeneous structures to pressure, temperature and stress is therefore of great interest to planetary scientists, materials scientists, physicists and chemists. X-ray computed tomography (XCT) is a powerful non-destructive method for imaging the internal structure of a sample and therefore analyzing heterogeneity of samples. XCT is widely applied to quenched samples; however, *in situ* characterizations at high pressure and temperature are critical in the cases of non-quenchable phases or dynamic studies where the ‘squeeze, cook and then look’ approach is not sufficient.

In XCT, the reconstructed three-dimensional image is computed from a series of two-dimensional X-ray radiographs. It is desirable for the reconstruction of a tomography image to acquire radiographs at small angular increments over 180° rotation with respect to an axis perpendicular to the incident X-ray beam. XCT at high pressure is usually performed using a static high-pressure press within which the anvils can be rotated under a uniaxial load transmitted by thrust bearings. This is the case of the setup at GeoSoilEnviro-CARS (GSECARS) of the Advanced Photon Source (Argonne National Laboratory, IL, USA) (Wang *et al.*, 2005) that uses either a Drickamer module or Paris–Edinburgh (PE) anvils, and the portable RoToPEC press (Álvarez-Murga *et al.*, 2017;



© 2018 International Union of Crystallography

Philippe *et al.*, 2016). Acquisition time for a tomogram in such an apparatus is mainly limited by the difficulty of transmitting the large axial load (50 tons in the case of the Drickamer within 250 tons hydraulic press, 450 tons for the RoToPEC) through the bearings to the rotating anvils. Typical acquisition times are of 20 min (in the RoToPEC) or higher. Another kind of setup includes the use of a conventional press, for example a compact panoramic PE press such as the one used at SPring-8, Japan (Urakawa *et al.*, 2010). A millimetric sample can be imaged within a 160° opening angle as the press frame blocks a 20° angular region. Reported scan times in monochromatic beam mode are of the order of 15 min (300 ms exposure time) for the quoted $12\ \mu\text{m}$ spatial resolution. This represents a faster acquisition time than the GSECARS system, and is roughly similar to that obtained using the RoToPEC, although at lower spatial resolution. A similar approach has been applied to diamond anvil cells (DACs), using a cross DAC with a high angular opening (150°) that adopts the principle of the ‘plate DAC’ (Boehler, 2006; Mao & Boulard, 2013; Wang *et al.*, 2012). In this case the very limited sample size ($<100\ \mu\text{m}$ diameter) requires the use of X-ray microscopy techniques to achieve a suitable spatial resolution (tens of nanometers). This greatly increases the acquisition time (hours per tomogram) and introduces further difficulties in terms of sample preparation and instrumental precision.

Current acquisition times of the order of minutes or tens of minutes per tomogram represent a significant limitation for dynamic studies of samples that evolve at a rate that is greater than or comparable with this acquisition time, or for samples which are mechanically unstable under high pressure and temperature conditions. For example, Fig. 1 shows the first and the last radiographs of a tomographic acquisition recorded in the RoToPEC of a partially liquid sample at high temperature and pressure. One can see the gap between the anvils which has closed significantly during the duration of the scan due to deformation and flow of the sample and environment. Because of the inhomogeneous deformation both in space and

time in the sample, an artefact-free reconstruction is impossible to achieve.

Recent developments in synchrotron tomography for materials science have greatly reduced the acquisition time that can be expected, and second or even sub-second tomography can now be considered routine for samples in *in situ* loading frames or other sample environments (Maire & Withers, 2014). Crystal monochromator optics on a synchrotron beamline typically transmit less than 0.1% of the incident spectrum, and so greatly decrease the flux available. For this reason, monochromatic beams are less suitable for dynamic studies. By using high-flux wide-bandwidth X-ray illumination, the exposure time per radiograph can be reduced accordingly. Fast detectors are also now capable of kHz frame rates (Schleppütz *et al.*, 2017). This enables increasingly fast dynamic processes to be studied *in situ* such as fracture, solidification or phase transformations (Baker *et al.*, 2012).

Here, we describe the recent development of fast X-ray imaging at high pressure and temperature at the Pressure, Structure and Imaging by Contrast at High Energy (PSICHE) beamline of Synchrotron Soleil, France. By combining the use of pink-beam illumination through a standard PE press in conjunction with the tomograph stage available at the PSICHE (King *et al.*, 2016), we have been able to significantly improve acquisition speed by at least 100 times compared with the current state of the art, even at high spatial resolution (pixel size $1.3\ \mu\text{m}$ with a true resolution of $3.3\ \mu\text{m}$ due to the beamline geometry). To demonstrate the potential of this device, we present a pilot study on silicate melt propagation through a solid matrix. New opportunities and on-going developments are given as final prospects.

2. X-ray imaging setup at the PSICHE beamline

We present below the main beamline characteristics needed for fast acquisition tomography scans at high pressure and

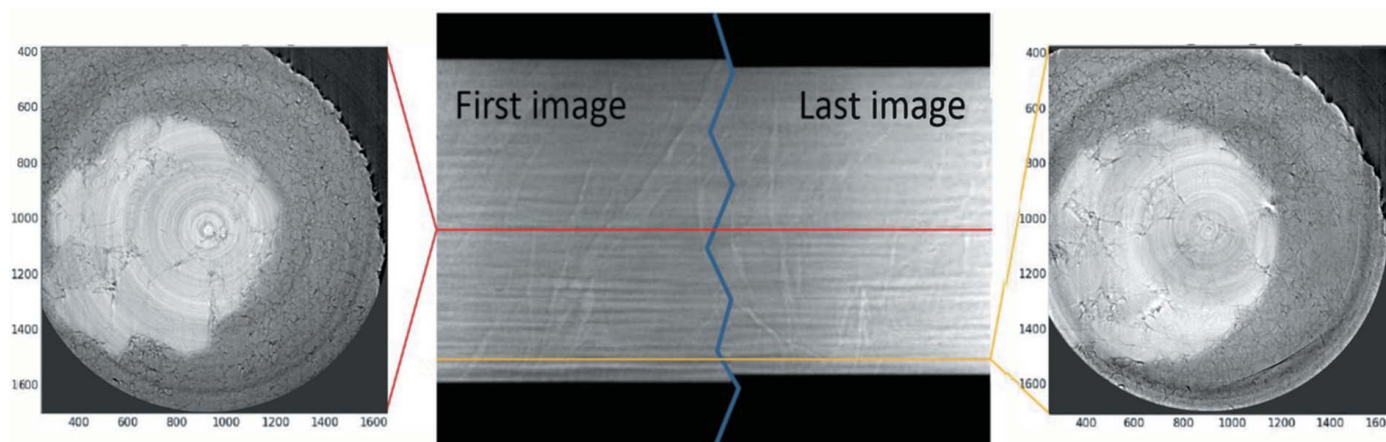


Figure 1

Center: first and last image of a tomogram recorded with a 20 min acquisition time in the RoToPEC apparatus at 3 GPa, 1800 K. The black areas at the top and bottom of the sample are due to the absorption from the PE anvils. One can see the opening gate between these anvils shortening upon the acquisition of the tomogram due to the flow of the sample and sample environment at these high temperatures. Attempted reconstructed slices are presented on the left and right, which present a large artefact because of the sample movement upon acquisition.

temperature. A detailed description of the specifications of the beamline can be found elsewhere (King *et al.*, 2016).

2.1. X-ray optics

The PSICHE beamline is based on a short straight section of the SOLEIL storage ring (Guignot *et al.*, 2013). An in-vacuum wiggler insertion device provides an intense broad-spectrum beam. Fixed cooled filters are used to remove the low-energy part of the spectrum, leaving a spectrum with a peak flux of around 25 keV (Dong *et al.*, 2011). In order to perform high-speed *in situ* tomography the beam spectrum is defined using combinations of filters in order to select a relatively wide energy bandwidth around a desired value ($\Delta E/E$ typically 0.1). Such an energy range constitutes a ‘pink beam’ which refers to the fact that a monochromator is not used to define the energy band spectrum. Instead, filters and an X-ray mirror act as high-pass and low-pass energy filters (King *et al.*, 2016; Rivers, 2016). Monochromatic beam is usually used in synchrotron beamlines in order to avoid beam hardening artefacts that are present in polychromatic laboratory instruments. However, a crystal monochromator on a synchrotron beamline typically transmits less than 0.1% of the beam. The beam flux at the sample position is around 3×10^{11} photons $s^{-1} mm^{-2}$ at 25 keV in monochromatic mode at PSICHE while it is 2×10^{15} photons $s^{-1} mm^{-2}$ in white-beam mode. Defining the beam energy spectrum with the X-ray mirror and absorption edges from filters and scintillator instead of a crystal monochromator therefore presents the advantage of working with a much higher flux while still eliminating beam-hardening artefacts from the reconstruction. The beam is sufficiently coherent and the bandwidth sufficiently low that propagation phase contrast can be used to increase contrast where attenuation contrast is limited (Paganin *et al.*, 2002). In order to optimize the absorption contrast, the mean beam energy is chosen depending of the sample composition and geometry so that typically 30% of the incident beam is transmitted. At PSICHE, mean beam energies can be selected between 25 and 85 keV using this approach (King *et al.*, 2016).

2.2. Tomograph stages

The PSICHE tomograph is based on a high-precision high-load-capacity Leuven Precision RT500 rotation stage and linear translation from LAB Motion Systems. It has a maximum load capacity of more than 50 kg, and is capable of rotating at 60 rpm with an eccentricity of <150 nm. All elements of the rotation stage including the granite table feature an open aperture of at least 250 mm to allow large samples or sample environments to be installed within the tomograph stage, below the sample position or to route cables and connectors to the sample. The large available space and load capacity makes it a very suitable base for *in situ* experiments requiring large or complicated sample environments such as in experiments with a PE press.

2.3. Detector

The detector uses a thin single crystal scintillator (YAG, LSO or LuAG) of 10 to 500 μm to convert the X-rays transmitted through the sample into a visible-light image. Microscope or other visible-light optics are used to form an image on a Hamamatsu Orca Flash4.0 sCMOS camera which allows full frame rates of up to 100 frames s^{-1} . Given a region of interest of 2048×512 pixels for reduced readout time, a full tomography dataset of 1500 radiographs can be recorded in 3.8 s. A mirror, inclined at 45° , is placed just behind the scintillator to reflect the visible light vertically. In this way, the optics and camera are not placed in the direct path of the X-ray beam, avoiding radiation damage to the electronics and minimizing darkening of the optics.

3. PE press setup at the beamline PSICHE

Fig. 2 shows the setup for the PE press at the PSICHE beamline. The current setup uses a conventional four-column PE press (Besson *et al.*, 1992) which allows working up to 10 GPa, 2000 K with conventional tungsten carbide anvils. It presents a 68.8° angular opening between the columns, and so a total useful angular opening of around 135° for tomography. This provides a total angular opening of about 135° upon a 180° rotation of the press. Once pressurized to its target pressure, the press is isolated from the hydraulic line

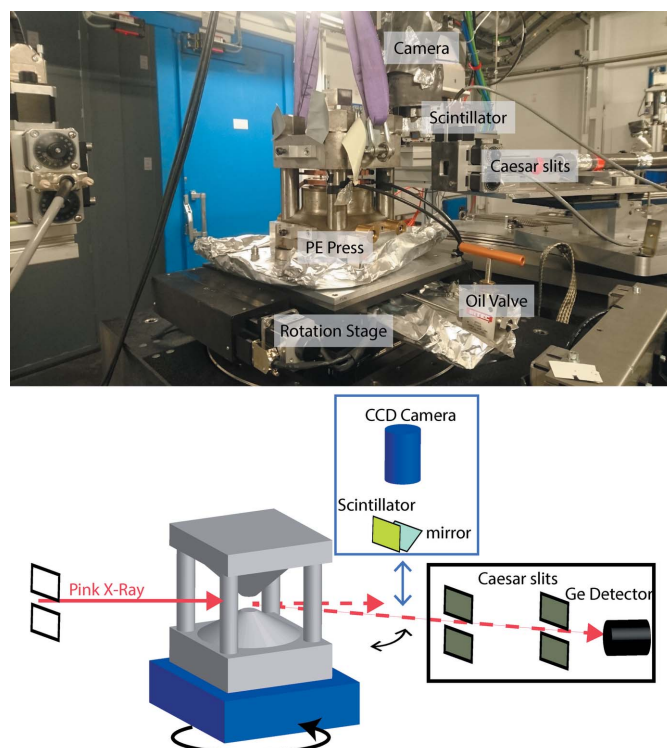


Figure 2 Photograph (top) and schematic drawing (bottom) of the PE press experimental setup at the PSICHE beamline at Synchrotron Soleil. The PE press is directly installed on the rotation stage for tomography. Both the Caesar diffraction setup and the camera setup can be brought in and out depending on whether one wants to work in diffraction or imagery mode.

connected to the press piston by closing a valve. The hydraulic line is then disconnected, allowing the press to rotate freely. High temperature is achieved by an alternating current power supply, and the anvils are continuously cooled using a flowing water circuit. Both the electrical cables and water hoses necessary for heating the sample and anvil cooling are routed through the hole in the rotation axis. In this way, 180° of rotation is possible without damaging the cables or connectors. As the electrical cables remain connected, the sample temperature can be controlled at constant pressure while imaging. A tomogram is recorded during a 180° rotation, after which the rotation returns to its starting position before the next tomogram. Eventually, a second tomogram could be recorded during the ‘rewind’ phase. This places some limits on the minimum time per tomogram, and interval between tomograms, due to the acceleration and deceleration times. In this operation mode, we have been able to record complete datasets in 10 s. This represents an improvement of around 100–1000 times with respect to the different systems discussed in the *Introduction*.

4. High pressure and temperature XCT experiments: rhyolite melt percolation through a solid silicate matrix

Understanding the manner in which fluids are distributed in partially molten rocks is critical to a variety of geophysical and geochemical phenomena. However, there are many unanswered questions regarding the physical processes involved in the generation of melts and their transportation through the mantle rocks. Recently, Zhu *et al.* (2011) demonstrated the exciting potential for three-dimensional micro-tomography to look at silicate-rich melts in contact with silicate-rich rocks in order to model melt transportation through mantle rocks. To our knowledge, until now percolation studies have been based on XCT imaging on recovered samples from quench experiments (*e.g.* Miller *et al.*, 2014, 2016). In the present work, we performed *in situ* fast XCT imaging. This avoids assumptions in the interpretation of quenched samples, and enables the study of the kinetics of percolation of melt. This is particularly important as melt percolation through silicate-rich rocks goes along with chemical and mechanical instabilities such as dissolution–precipitation reactions between the mantle and the percolating melt that lead to the formation of high-permeability channels due to a positive feedback between melt flow and reaction (Pec *et al.*, 2015, 2017; King *et al.*, 2010).

Starting materials consisted of a mixture of finely ground natural rhyolitic magmatic rock and roughly ground San Carlos olivine crystals as a solid silicate matrix. Fe–Mg-rich olivine [(Mg_{0.9}, Fe_{0.1})₂SiO₄] was chosen in order to obtain sufficient absorption contrast between the rhyolite and the solid silicate and facilitate their identification. The rhyolitic powder and olivine crystals were thoroughly mixed in order to obtain a homogeneous mixture. The PE cell assembly used for these experiments is represented in Fig. 3. It consists of a center disc of X-ray transparent boron epoxy (BE). Above and below the BE discs are ZrO₂ caps, insuring excellent

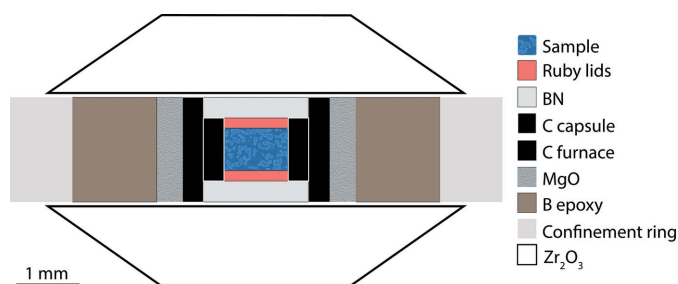


Figure 3
PE assemblage used for the present percolation experiments.

thermal insulation and preventing temperature gradients within the sample. The sample is heated using a graphite furnace with Mo foil leads. The composite BE/ZrO₂ experimental assembly design is optimized to provide a higher temperature range, to increase the accessible window between the WC anvils at high P–T conditions, and for longer cell stability at elevated pressure and temperature compared with the standard BE gasket (Kono *et al.*, 2014). The sample is contained in a X-ray transparent graphite capsule. MgO insulating material is placed between the graphite heater and boron epoxy to avoid reactions and increase stability with time (Kono *et al.*, 2014).

Radiographic imaging of the sample in the cell assembly was performed using the PSICHE tomography detector. A visible-light image was formed using a 90 µm-thick YAG scintillator screen and transmitted to the Hamamatsu ORCA Flash4.0 sCMOS camera using a 5× microscope objective, giving an effective pixel size of 1.3 µm. The energy profile of the pink beam used for these experiments is presented in Fig. 4. The energy bandwidth is about 4 keV. A tomographic dataset consisted of 700 projections with 10 ms exposure time for each image. Thus, each tomogram has a ‘collection time’ of about 10 s. In addition, reference images were recorded before and after the projections. A series of tomograms were

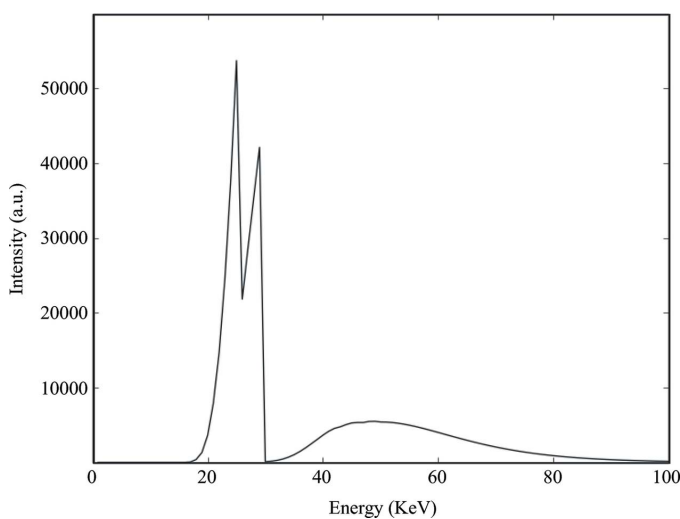


Figure 4
Energy profile of the ‘pink beam’ after energy filtering as used for imaging at high speed in the present experiments.



Figure 5 Reconstructed slice of a mixture of ground rhyolite together with olivine grains at 3 GPa and 1100 K (a), 1600 K (b) and after a few minutes at 1600 K (c).

acquired with 10 s collection time combined with 5 s intervals between scans. Reconstructions sections of the sample are performed using standard filtered backprojection in PyHST2, employing Paganin phase retrieval (Mirone *et al.*, 2014; Paganin *et al.*, 2002).

The sample was first pressurized to 3 GPa and then heated progressively. Fig. 5 shows reconstructed vertical sections through the sample, parallel to the press axis. Above 1100 K, strong deformation of the sample chamber is observed as its volume is reduced drastically due to melting of the rhyolite material (Fig. 5a). In a few minutes and with increasing temperature the melt reorganized itself toward the border of the capsule. When the temperature reached 1600 K, we observed rapid and progressive demixing of liquid iron from the melt that precipitated as iron metallic spherules, probably due to the reduction of iron in the melt by the graphite capsule. At the same time, gas bubbles formed in the interior of the sample (Figs. 5b and 5c).

In order to estimate the effect of both the limited angle opening view and the reconstruction algorithm, we present reconstructed sections from *ex situ* measurements (where the sample is outside the PE press) and *in situ* measurements (the sample is within the PE press) by means of either filtered back projection (FBP) or the algebraic reconstruction technique (ART) in Fig. 6. The restricted angle availability (135°) for *in situ* imaging produces artefacts which are particularly noticeable where strongly attenuating material is present, as the artefacts are proportionally strong. This is the case in the present experiment as we observed the precipitation of metallic iron beads within the sample. Reconstructions were first performed by the use of the FBP algorithm. The FBP method is an analytical algorithm that is fast in

calculation time; however, it is sensitive to noise and small number of projections. It is based on the Fourier transform theory, and on the assumption that both the measurement process and the projection data are represented by a continuous function. In these reconstructions sections of the sample

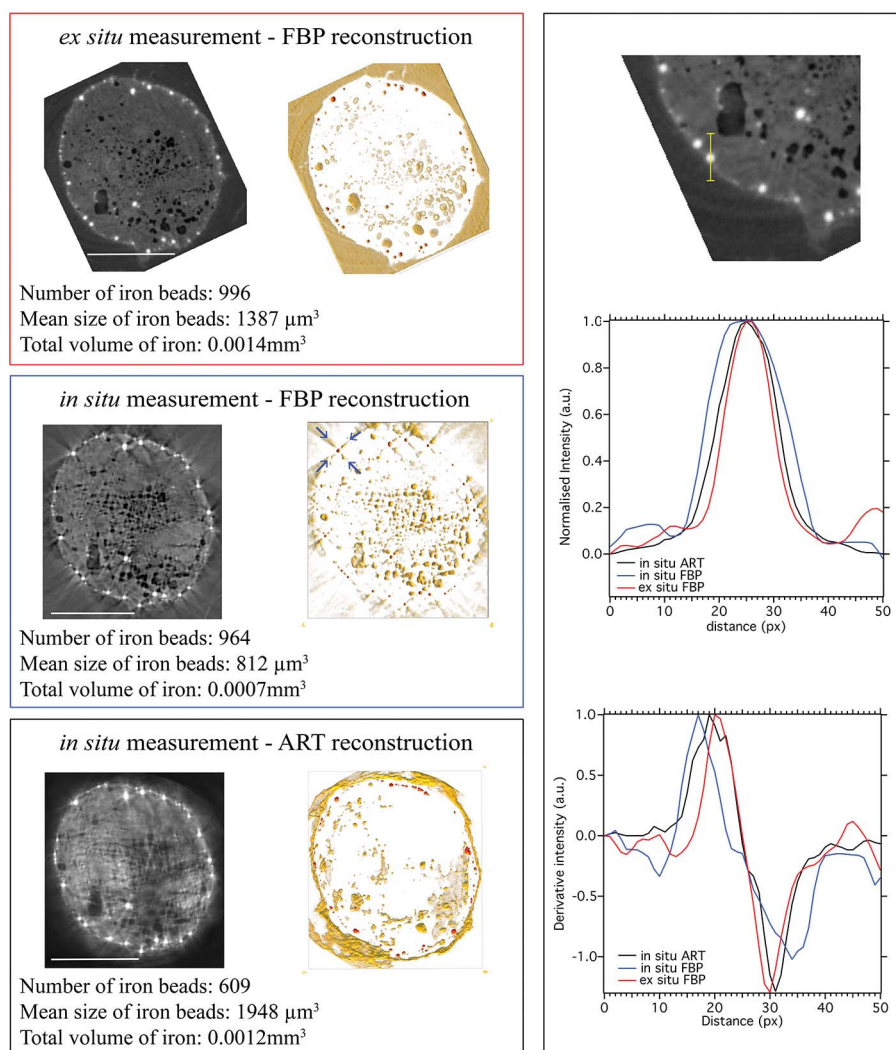


Figure 6 Evaluation of the effect of the missing angles, and the choice of algorithm for the reconstruction. Left: reconstructed images of the sample at room pressure and temperature after the experiments and analyses of the iron beads. Top: from a tomogram collected *ex situ*, outside the PE press and reconstructed by the mean of FBP algorithm; middle: from a tomogram collected *in situ* and reconstructed by the mean of FBP algorithm; bottom: reconstructed by the mean of ART algorithm. Right: analyses of the sharpness of the images by measuring the intensity profile and their first derivative. The red line in the image at the top indicates the profile line used for the analyses. The white scale bars represent 500 μm.

one can see streaking around these beads along the directions which are obscured by the columns of the press (highlighted by the blue arrows on Fig. 6). These contrasts could be misinterpreted as gas/empty space and be problematic for studies on magma degassing, for example. In order to overcome this issue the data were reprocessed using an ART algorithm with ten iterations, from the *TXM-Wizard* software package (Liu *et al.*, 2012). The ART method treats the problem of image reconstruction as a discrete problem from the start. Any image will be constructed inside a rectangular grid of picture elements, or pixels. The ART method is an iterative algorithm based on linear algebra and matrix theory. ART is slower but better adapted for a small number of projections (Wang *et al.*, 2012; Gordon *et al.*, 1970). As presented in Fig. 6, no more artefacts are observed around the metallic iron beads and, as demonstrated by the intensity profiles, images are sharper when reconstructed with the ART algorithm and the FBP. Although we noticed that contrast between the rhyolite and olivine becomes weaker with the number of iterations, reconstruction of a scan collected on the sample at high pressure and temperature shows it is still possible to segment the melt from the solid olivine (Fig. 7). Examples of analyses of the iron beads using Fiji's particle analyses option are also presented in Fig. 6. While the total amount of iron is similar in all three volume reconstructions, the choice of FBP or ART reconstruction algorithm influences the resolution and therefore the number of iron beads and their mean size: the ART did not allow resolving beads that are close to each other.

Understanding melt extraction and transportation will provide important knowledge on magmatic processes and chemical differentiation in the Earth's interior. For example, it is considered that the metallic core of the Earth is formed from extensively molten silicate layer (magma ocean) on the Earth's surface (Rubie *et al.*, 2003; Wood *et al.*, 2006). The first process of this model involves separation of liquid metal from silicate melt, with the metal droplets then falling into the magma ocean. High-pressure X-ray imaging may enable us to simulate these processes at the high-pressure and high-temperature conditions of the Earth and planetary interiors and provides important knowledge on understanding the core formation process in the magma ocean model (Shi *et al.*, 2013).

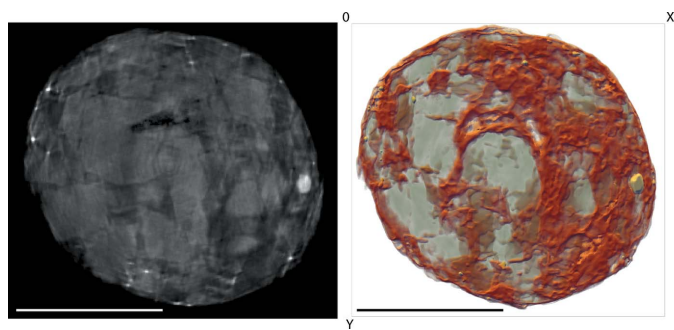


Figure 7
Reconstructed slice of the sample at 3 GPa and 1600 K and volume rendering of the melt distribution (in brown) in the volume. The iron beads are represented in yellow. The scale bar represents 500 μm .

By adding the fourth dimension 'time', one can now study the dynamics of deep Earth processes such as melt percolation velocity or crystallization rates, as well as the vesiculation rate of the melt, another important parameter in magmatic processes. Naturally, fast tomography at high pressure will also find applications in other scientific field such as chemistry, physics and material sciences.

5. Future developments: the UToPEC

Based on these first results, a new high-pressure device optimized for high-speed tomography at the PSICHE beamline has been designed and is under construction. This new device will allow working up to 15 GPa and 2000 K.

In order to increase the quality of the reconstructed images, the angular opening will be maximized using a two-column system, based on a modified VX press (Klotz *et al.*, 2004). As presented in Fig. 8, it will offer a 165° angular opening in order to reduce the reconstruction artefacts currently observed. The extra 30° of the opening will significantly reduce the reconstruction artefact presented in Fig. 6. The press will also have a smaller diameter than the current four-column system (170 mm *versus* 250 mm) which will allow a smaller sample detector distance to be used. This is particularly important, as the limiting spatial resolution will deteriorate with increasing sample–detector distance. This is due to the penumbral blurring caused by the source size, and also the fringes caused by phase contrast effects, which while providing edge enhancement contrast also have the effect of decreasing the spatial resolution. Given the geometry of the beamline, the actual true spatial resolution is limited by the source size. A future upgrade to the SOLEIL storage ring, which would reduce the



Figure 8
Schematic of the new design of a PE press optimized for *in situ* imaging. This press is significantly smaller (170 mm diameter) and presents a wider opening of 165° which will allow a higher quality of imaging. A rotary union is used for the water-cooling system as well as the electrical wiring. This will allow acquisition upon continuous rotation at a fixed pressure reducing the acquisition time of a tomogram.

effective size of the X-ray source, will allow a true spatial resolution to below 1.6 μm at 60 keV, limited in this case by the phase contrast fringes.

In order to study processes such as degassing processes of magma, faster acquisition time is needed (<1 s). To do so, a system of rotary couplings will be used to bring the electrical heating power and the cooling water to the press. As stated previously, the acquisition time for the use of a standard PE press is currently limited by the requirement to rewind the stage, thus a continuous rotation stage will reduce the acquisition time. A quick-release fitting will be used to connect the hydraulic line to the press. Once the hydraulic line is removed, continuous rotation will be possible. With this improvement, it will be possible to acquire a full tomogram in 0.5 s, corresponding to the maximum rotation speed of the stage. This is a further factor of ten compared with the current instrument, and a factor of 1000 compared with the reported state of the art.

The characteristics and capacity of the three different presses are listed in Table 1. Depending on the necessity for experiments, one user will be able to use one or the other. For example, the RoToPEC press is necessary for imaging upon deformation studies while the UToPEC will be necessary for the study of fast processes.

Finally, one should note that the PSICHE beamline offers the possibility to perform simultaneous white-beam energy-dispersive diffraction and pink-beam X-ray tomography. These two techniques are very complementary in material science. For example, tomographic reconstruction or two-dimensional radiography can be used to target a diffraction measurement in a heterogenous sample, and X-ray diffraction can be used for phase identification, measurement of the strain, pressure or crystal orientation during a tomographic experiment. Changing between the tomography and diffraction modes can be performed simply by changing the beam filters, and defining the incident beam with slits just upstream of the sample (Fig. 2).

6. Conclusions

In this article, we have shown that by combining a standard PE press mounted on a suitable synchrotron tomograph with the use of pink-beam illumination it is possible to obtain a very large improvement in temporal resolution for tomography at high pressure and temperature compared with current systems. A large range of evolving systems at high pressure and temperature become accessible for investigations using *in situ* tomography. The drawback when using a standard press is reconstruction artefacts arising from the limited angular opening of the press. We describe a modified press, optimized for high-speed tomography, which will allow a further order of magnitude improvement in speed, while simultaneously minimizing these reconstruction artefacts.

Table 1
Characteristics and capacity of the three different presses discussed.

Press	Description	Angle range of view	Acquisition time	Advantages
RoToPEC	Rotational anvils	180°	10–20 min	High-quality imaging, possibility to perform deformation experiments
Standard PE	Four-column PE press placed on a rotation stage	135°	10 s	
UToPEC	Two-column PE press placed on a rotation stage	165°	<1 s	Ultrafast imaging at high pressure and temperature

Acknowledgements

We acknowledge the Soleil synchrotron radiation facility for the allocation of beam time (proposal No. 99160122). The construction of the new PE press is supported by the Region île de France DIM OxyMORE grant. This paper was improved by the thorough and constructive comments and suggestions from Yanbin Wang and an anonymous reviewer.

References

- Álvarez-Murga, M., Perrillat, J. P., Le Godec, Y., Bergame, F., Philippe, J., King, A., Guignot, N., Mezouar, M. & Hodeau, J. L. (2017). *J. Synchrotron Rad.* **24**, 240–247.
- Baker, D. R., Brun, F., Shaughnessy, C. O., Mancini, L., Fife, J. L. & Rivers, M. (2012). *Nat. Commun.* **3**, 1135–1137.
- Besson, J. M., Hamel, G., Grima, T., Nelmes, R. J., Loveday, J. S., Hull, S. & Häusermann, D. (1992). *Int. J. High. Press. Res.* **8**, 625–630.
- Boehler, R. (2006). *Rev. Sci. Instrum.* **77**, 1–4.
- Dong, X., Moreno, T., Guignot, N. & Itié, J.-P. (2011). *Proc. SPIE*, **8141**, 814113.
- Gordon, R., Bender, R. & Herman, G. T. (1970). *J. Theor. Biol.* **29**, 471–481.
- Guignot, N., Itié, J.-P., Zerbino, P., Delmotte, A. & Moreno, T. (2013). *2013 AGU Fall Meeting Abstracts*. American Geophysical Union.
- King, A., Guignot, N., Zerbino, P., Boulard, E., Desjardins, K., Bordessoule, M., Leclercq, N., Le, S., Renaud, G., Cerato, M., Bornert, M., Lenoir, N., Delzon, S., Perrillat, J.-P., Legodec, Y. & Itié, J.-P. (2016). *Rev. Sci. Instrum.* **87**, 93704.
- King, D. S. H., Zimmerman, M. E. & Kohlstedt, D. L. (2010). *J. Petrol.* **51**, 21–42.
- Klotz, S., Hamel, G. & Frelat, J. (2004). *High. Press. Res.* **24**, 219–223.
- Kono, Y., Park, C., Kenney-Benson, C., Shen, G. & Wang, Y. (2014). *Phys. Earth Planet. Inter.* **228**, 269–280.
- Liu, Y., Meirer, F., Williams, P. A., Wang, J., Andrews, J. C. & Pianetta, P. (2012). *J. Synchrotron Rad.* **19**, 281–287.
- Maire, E. & Withers, P. J. (2014). *Int. Mater. Rev.* **59**, 1–43.
- Mao, W. L. & Boulard, E. (2013). *Rev. Miner. Geochem.* **75**, 423–448.
- Miller, K. J., Zhu, W., Montési, L. G. J. & Gaetani, G. A. (2014). *Earth Planet. Sci. Lett.* **388**, 273–282.
- Miller, K. J., Zhu, W., Montési, L. G. J., Gaetani, G. A., Le Roux, V. & Xiao, X. (2016). *J. Geophys. Res. Solid Earth.* **121**, 5776–5793.
- Mirone, A., Brun, E., Gouillart, E., Tafforeau, P. & Kieffer, J. (2014). *Nucl. Instrum. Methods Phys. Res. B*, **324**, 41–48.
- Paganin, D., Mayo, S. C., Gureyev, T. E., Miller, P. R. & Wilkins, S. W. (2002). *J. Microsc.* **206**, 33–40.
- Pec, M., Holtzman, B. K., Zimmerman, M. & Kohlstedt, D. L. (2015). *Geology*, **43**, 575–578.
- Pec, M., Holtzman, B. K., Zimmerman, M. & Kohlstedt, D. L. (2017). *J. Petrol.* **58**, 979–1003.

- Philippe, J., Le Godec, Y., Mezouar, M., Berg, M., Bromiley, G., Bergame, F., Perrillat, J. P., Alvarez-Murga, M., Morand, M., Atwood, R., King, A. & Régnier, S. (2016). *High. Press. Res.* **36**, 512–532.
- Rivers, M. (2016). *SPIE Newsroom*, pp. 1–3. doi:10.1117/2.1201608.00674.
- Rubie, D. C., Melosh, H. J., Reid, J. E., Liebske, C. & Righter, K. (2003). *Earth Planet. Sci. Lett.* **205**, 239–255.
- Schlepütz, C. M., Mokso, R., Theidel, G., Billich, H., Schmid, E., Celcer, T., Mikuljan, G., Marone, F., Schlumpf, N. & Stampanoni, M. (2017). *Proceedings of the Third International Conference on Tomography of Materials and Structures (ICTMS2017)*, Lund, Sweden, 26–30 June 2017, p. 162.
- Shi, C. Y., Zhang, L., Yang, W., Liu, Y., Wang, J., Meng, Y., Andrews, J. C. & Mao, W. L. (2013). *Nat. Geosci.* **6**, 1–5.
- Urakawa, S., Terasaki, H. P., Funakoshi, K., Uesugi, K. & Yamamoto, S. (2010). *J. Phys. Conf. Ser.* **215**, 12026.
- Wang, J., Yang, W., Wang, S., Xiao, X., De Carlo, F., Liu, Y. & Mao, W. L. (2012). *J. Appl. Phys.* **111**, 112626.
- Wang, Y., Uchida, T., Westferro, F., Rivers, M. L., Nishiyama, N., Gebhardt, J., Leshner, C. E. & Sutton, S. R. (2005). *Rev. Sci. Instrum.* **76**, 073709.
- Wood, B. J., Walter, M. J. & Wade, J. (2006). *Nature (London)*, **441**, 825–833.
- Zhu, W., Gaetani, G. A., Fusses, F., Montési, L. G. & De Carlo, F. (2011). *Science*, **332**, 88–91.